AIP | The Journal of Chemical Physics

Alkali metal mediated C–C bond coupling reaction

Hiroto Tachikawa

Citation: The Journal of Chemical Physics **142**, 064301 (2015); doi: 10.1063/1.4906944
View online: http://dx.doi.org/10.1063/1.4906944
View Table of Contents: http://scitation.aip.org/content/aip/journal/jcp/142/6?ver=pdfcov
Published by the AIP Publishing

Alkali metal mediated C–C bond coupling reaction

Hiroto Tachikawa[a)]
Division of Materials Chemistry, Graduate School of Engineering, Hokkaido University, Kita-ku, Sapporo 060-8628, Japan

(Received 14 October 2014; accepted 16 January 2015; published online 9 February 2015)

Metal catalyzed carbon-carbon (C–C) bond formation is one of the important reactions in pharmacy and in organic chemistry. In the present study, the electron and hole capture dynamics of a lithium-benzene sandwich complex, expressed by $Li(Bz)_2$, have been investigated by means of direct *ab-initio* molecular dynamics method. Following the electron capture of $Li(Bz)_2$, the structure of $[Li(Bz)_2]^-$ was drastically changed: Bz–Bz parallel form was rapidly fluctuated as a function of time, and a new C–C single bond was formed in the C_1–C_1' position of Bz–Bz interaction system. In the hole capture, the intermolecular vibration between Bz–Bz rings was only enhanced. The mechanism of C–C bond formation in the electron capture was discussed on the basis of theoretical results. © *2015 AIP Publishing LLC*. [http://dx.doi.org/10.1063/1.4906944]

I. INTRODUCTION

Transition metal catalyzed carbon-carbon (C–C) bond formation reaction is one of the most powerful methods in synthetic organic chemistry.[1–5] Especially, the cross-coupling reactions have provided a great impetus to modern organic synthesis. According to the proposed mechanisms of these cross-coupling reactions,[6–10] the reaction is initiated by the oxidative insertion of palladium (0) into a carbon-halogen bond of the aryl halide used as substrate and forming a palladium (II) intermediate. This key step is followed by the coupling of reactants, reductive elimination of the newly formed coupled product, and regeneration of the palladium (0) center. For these cross-coupling reactions, ligands with soft donor sites are often required in order to stabilize the palladium (0) state and also to satisfy the vacant coordination sites of the palladium (II) intermediate. Bulky arylphosphines are particularly popular as soft ligands for these reactions. Thus, the multiple steps need to obtain the C–C bond formation.

In the present study, the electron and hole capture processes of lithium-benzene sandwich complex $Li(Bz)_2$ were investigated by means of direct *ab-initio* molecular dynamics (AIMD) method.[11–13] The reactions are expressed by

$$Li(Bz)_2 + e^- \rightarrow [Li^-(Bz)_2]_{ver} \rightarrow \text{product},$$
$$Li(Bz)_2 + \text{hole} \rightarrow [Li^+(Bz)_2]_{ver} \rightarrow \text{product},$$

where $[Li^+(Bz)_2]_{ver}$ means a transient $Li^+(Bz)_2$ species formed at a vertical electron capture and ionization point from $Li(Bz)_2$. We found that the C–C bond formation reaction directly proceeds after the electron capture of $Li(Bz)_2$.

Charge and discharge processes of lithium in graphite layer are of considerable interest because the processes are correlated strongly with the nature of lithium secondary battery.[14] The $Li^+(Bz)_2$ complex is the smallest sized-model of Li-graphite systems. The structures and electronic states of the complexes are the topics of several gas phase experiments[15–17] and computational studies.[18–22]

Amicangle and Armentrout determined a lithium affinity of benzene molecule using threshold collision—induced dissociation method: $Li^+ + C_6H_6 \rightarrow Li^+(C_6H_6) + 1.67 \pm 0.14$ eV. The computational studies indicate that the lithium affinity of C_6H_6 (denoted by Bz) is calculated in the range of 1.40-1.90 eV.[17,19,20,22]

In two graphene layers, dissociation energy of Li^+ from $Li^+(Bz)_2$, $Li^+(Bz)_2 \rightarrow Li^+ + 2(Bz)$, was experimentally measured to be 2.75 ± 0.21 eV. Vollmer *et al.* calculated the dissociation energy of $Li^+(Bz)_2$ to be 2.67 eV at the G3(MP2) level.[23] In case of Li atom, the dissociation energy was calculated to be 0.85 eV. The layer distances of $Li(C_6H_6)$ and $Li^+(Bz)$ are 4.504 and 3.842 Å, respectively. Denis and Iribarne investigated the interaction system of benzene-Lithium 1:1 complexes using *ab initio* calculations. They found that benzene-Li 1:1 complex has two electronic states: ionic and non-ionic states. The ionic state is 1.8 kcal/mol lower in energy than that of non-ionic state.[24] Thus, the static structures and electronic structures of $Li(Bz)_2$ systems are well understood experimentally and theoretically.[25] However, details of charge and discharge processes are scarcely known. Therefore, the investigation of the reaction dynamics of $Li(Bz)_2$ provides information on the charge-discharge process of lithium battery.

II. METHOD OF CALCULATION

Static *ab-initio* calculations were carried out using Gaussian 09 program package using 6-31+G(d), 6-311G(d,p), 6-311++G(d,p), and 6-311++G(3df,3pd) basis sets.[26] The geometries and energies were obtained by Møller–Plesset perturbation (MP2) theory and the long range corrected version of B3LYP using the Coulomb-attenuating (CAM-B3LYP) methods. The atomic charge was calculated by means of natural population analysis (NPA) method. Self consistent reaction field (SCRF) method was applied to the energy

a)Author to whom correspondence should be addressed. Electronic mail: hiroto@eng.hokudai.ac.jp. Fax: +81 11706-7897.

TABLE I. Optimized parameters of $Li(Bz)_2$ and total energies (E_{total} in a.u.) calculated at several levels of theory. Bond lengths and angles are in Å and in degrees, respectively.

Parameter	MP2/6-311++G(d,p)	MP2/6-31+G(d)	CAM-B3LYP/6-311++G(d,p)	CAM-B3LYP/6-311G(d,p)	CAM-B3LYP/6-311++G(3df,3pd)
R_1	3.633	3.599	3.730	3.715	3.733
R_2	3.633	3.599	3.730	3.715	3.733
R_3	2.299	2.294	2.331	2.320	2.330
θ	104.4	103.3	106.3	106.3	106.5
E_{total}	−470.6418	−470.4081	−471.8317	−471.7807	−471.8697

calculation of solute of $Li(Bz)_2$ in the presence of solvents to estimate the solvation energy.

In the direct AIMD calculation,[27–30] first, the geometry of neutral $Li(Bz)_2$ was optimized at the CAM-B3LYP/6-311G(d,p) level. From the optimized geometry, we carried out the direct AIMD calculation under constant total energy condition. In addition to the trajectory from the equilibrium point, we generated geometries around the equilibrium point randomly and selected 10 geometries with the energy difference lower than 1.0 kcal/mol from the equilibrium point of $Li(Bz)_2$. First, we generated randomly several geometries around the equilibrium geometry. Next, the total energies and energy difference from the equilibrium point were calculated. Among them, the ten geometries having smaller energy difference than 1.0 kcal/mol were selected.

The trajectories on the ionic state potential energy surfaces were run on the assumption of vertical ionization or vertical electron capture from the neutral state. The trajectory calculations of the ionic states were performed under constant total energy condition at the CAM-B3LYP/6-311G(d,p) level. The equation of motion was solved by the velocity Verlet algorithm with a time step of 0.2 fs. The drifts of total energies

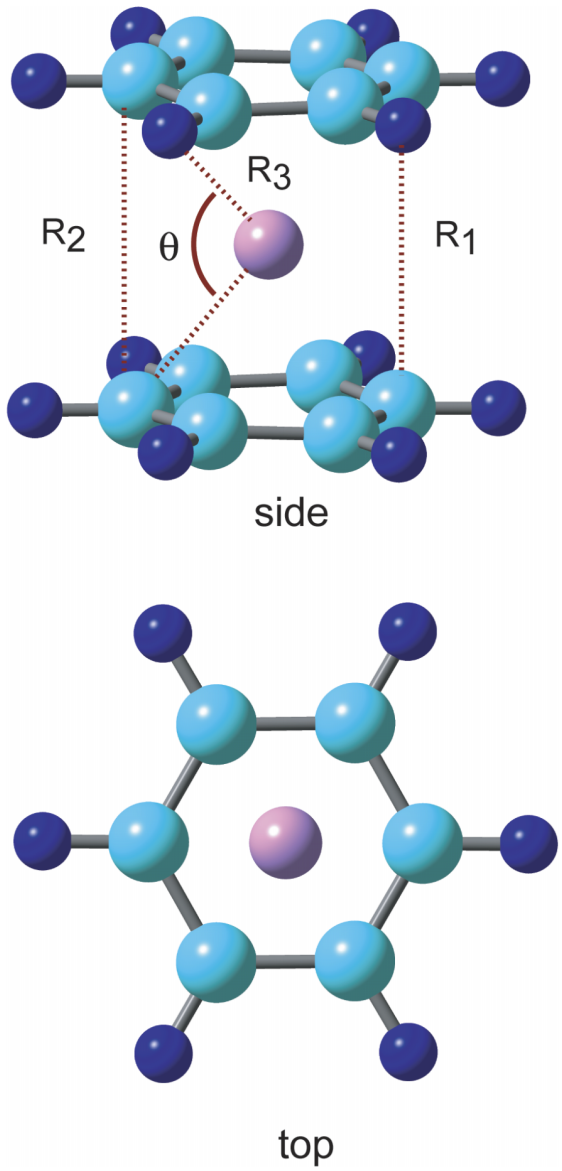

FIG. 1. Structure and geometrical parameters of $Li(benzene)_2$ complex calculated at the MP2/6-311++G(d,p) level.

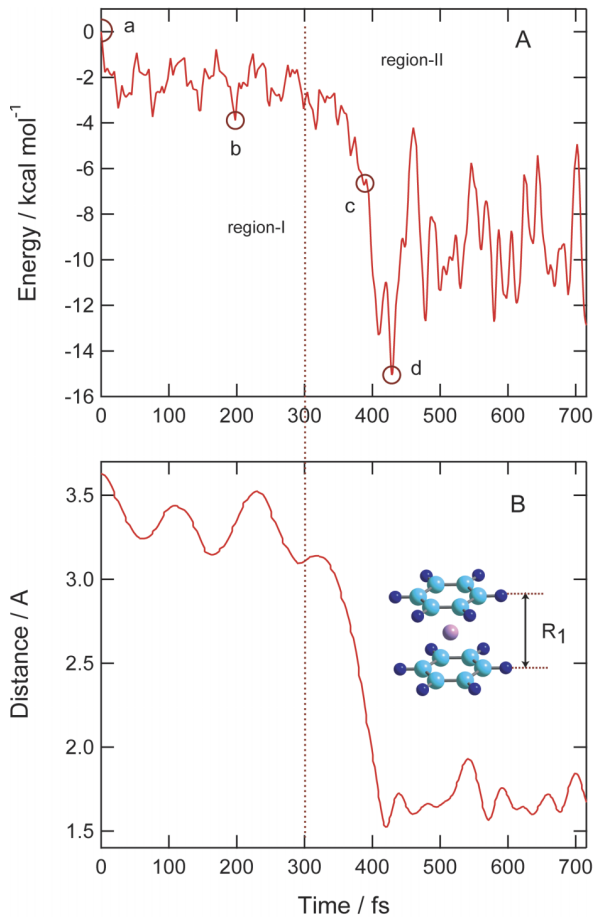

FIG. 2. Time evolutions of (a) potential energy of $Li^-(benzene)_2$ and (b) C–C bond distance between benzene rings (R_1) following vertical electron capture from neutral state calculated as a function of time.

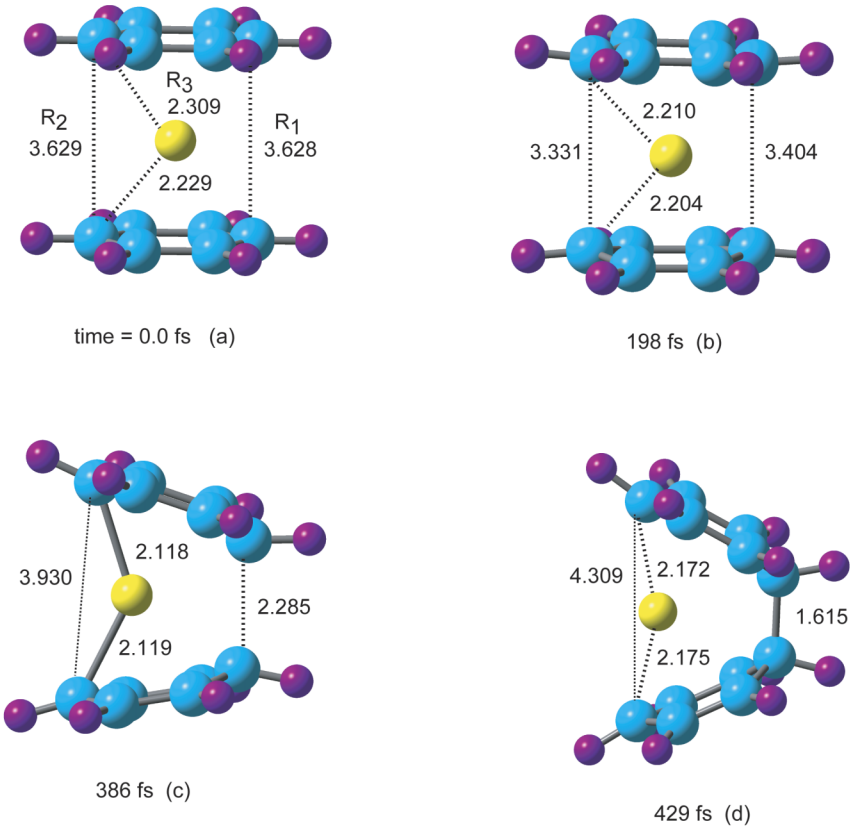

FIG. 3. Snapshots of $Li(benzene)_2^-$ following vertical electron capture from neutral state. Values mean interatomic distances (in Å).

were less than 1.0×10^{-2} kcal/mol in all of the trajectory calculations. No symmetry restriction was applied to the calculation of the energy gradients. The AIMD calculations were carried out using handmade code developed by our group.

III. RESULTS

A. Structure of $Li(Bz)_2$ neutral complex

First, the sandwich complex of $Li(Bz)_2$ was fully optimized at the several levels of theory. The optimized geometrical parameters are given in Table I, while the structure obtained at the MP2/6-311++G(d,p) level is given in Figure 1. The carbon-carbon distances between benzene rings were close to $R_1 = R_2 = 3.633$ Å at the MP2/6-311++G(d,p) level. The other level of theory gave the similar geometrical parameters. The distance of Li from the carbon atom of Bz is 2.299 Å.

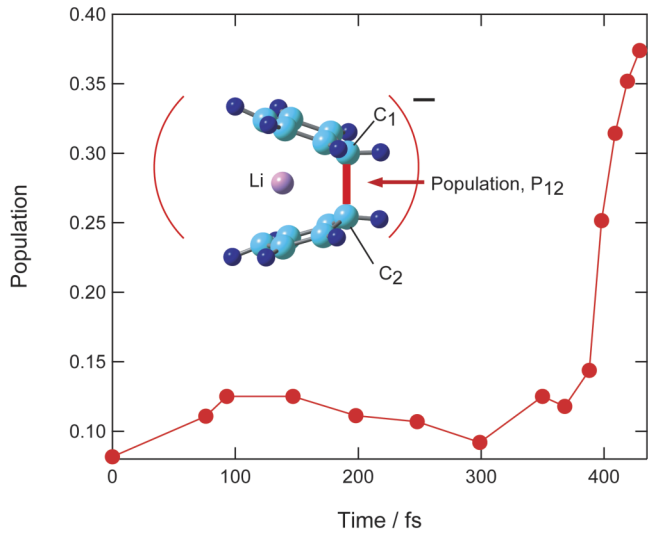

FIG. 4. Time evolutions of C–C bond population formation between benzene rings (P_{12}) following vertical electron capture from neutral state.

B. Electron capture dynamics

Time propagation of potential energy of the system $(Li^-(Bz)_2)$ following the electron capture is given in Figure 2. After the electron capture of $Li(Bz)_2$, the energy decreased rapidly to −1.8 kcal/mol at 5 fs due to the rapid structural stabilization of $Li^-(Bz)_2$. Immediately, the energy fluctuated periodically with the time period of 55 fs.

The reaction dynamics of $[Li^-(Bz)_2]_{ver}$ can be divided into two time regions (see dotted line in Fig. 2): one is a time region from zero to 300 fs and that from 300 to 700 fs. At the first time region from zero to 300 fs (denoted by region-I), the structure of $Li^-(Bz)_2$ fluctuated as keeping the sandwich structure, while the distance between rings (R_1) fluctuated periodically with vibrational energy of 330 cm^{-1} after the electron capture. After 300 fs (region-II), the potential energy and inter-plane distance were suddenly changed: potential energy is changed from −3.5 to −15.5 kcal/mol, and the inter-plane distance (R_1) was shortened from 3.0 to 1.5 Å. This drastic change is caused by the single C–C bond formation between two benzene rings. Thus, the potential energy was drastically changed at time region from 300 to 400 fs. At 420 fs, the energy reached to its lowest point (point **d**).

The time evolution of bond distance between benzene rings (R_1) is given in Fig. 2(b). The inter-plane distance of

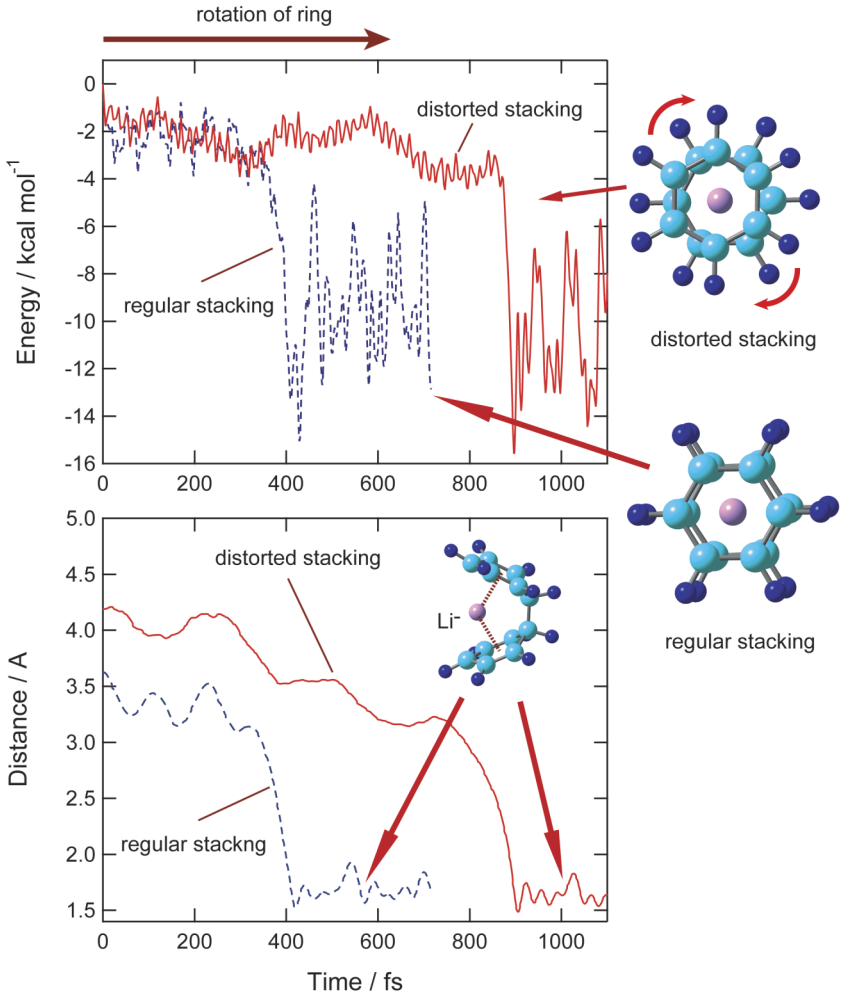

FIG. 5. Effects of initial structures on the reaction time of the C–C bond formation.

$Li(Bz)_2$ was 3.628 Å at time zero. After the electron capture, the distance varied with a time period of 100 fs, and the amplitude was 0.25 Å. At 320 fs, the benzene rings approached each other, and then the distance reached 1.50 Å at 420 fs. This drastic change indicates that a new C–C single bond is spontaneously formed after the electron capture of $Li(Bz)_2$.

Snapshots of $Li^-(Bz)_2$ following the electron capture of neutral system are illustrated in Figure 3. The structure at time zero corresponds to $[Li^-(Bz)_2]_{ver}$ (the structure at the vertical point). The intermolecular distances were $R_1 = 3.628$ Å, $R_2 = 3.629$ Å, and $R_3 = 2.309$ Å. The NPA charges on Li, $(Bz)_a$, and $(Bz)_b$ were +0.58, −0.79, and −0.79, respectively. This result indicates that an excess electron is mainly distributed on the benzene rings. At time = 198 fs (point **b**), the distances of C–C bond were slightly shortened ($R_1 = 3.404$ Å and $R_2 = 3.331$ Å). However, the whole structure of $Li(Bz)_2$ was close to that at time zero.

The structure of $Li^-(Bz)_2$ was drastically changed at 386 fs (point **c**): the C–C bond distances were $R_1 = 2.285$ Å and $R_2 = 3.930$ Å, and the C–Li distance was $R_3 = 2.118$ Å. At final stage of the reaction (429 fs), the C–C single bond was newly formed as the geometrical parameters ($R_1 = 1.615$ Å, $R_2 = 4.309$ Å, and $R_3 = 2.172$ Å). The dynamics calculation showed that the new C–C bond (R_1) is spontaneously formed by the electron capture of $Li(Bz)_2$ at the equilibrium point.

Time evolution of bond population between C_1 and C_2 atoms (P_{12}) is given in Figure 4. At time zero, the population P_{12} was close to zero (0.08). At time region-I (0-300 fs), P_{12} was almost constant and was small value ($P_{12} = 0.08$-0.13). The value of P_{12} increased suddenly from 300 to 430 fs and reached to $P_{12} = 0.37$ at final stage of reaction (430 fs). These results indicate that the C–C single bond is directly formed after the electron capture of $Li(Bz)_2$.

C. Effects of initial structures on the reaction dynamics

In Secs. I and II, the regular stacking form of $Li(Bz)_2$ was considered as the initial structure in the direct AIMD calculation. In this section, a distorted stacking form of $Li(Bz)_2$ was examined to elucidate the effects of distorted angle from the regular stacking form on the reaction time. Figure 5 (right) shows the structures of regular and distorted stacking forms of $Li(Bz)_2$. In the distorted stacking form, the distorted angle between benzene rings is 30° shifted from each other as shown in Figure 5 (C_2 symmetry).

The results of electron capture dynamics of distorted stacking form were given in Figure 5. The result of the regular stacking form is plotted by dashed curve for comparison. The new C–C bond was formed at 400 fs in the regular stacking

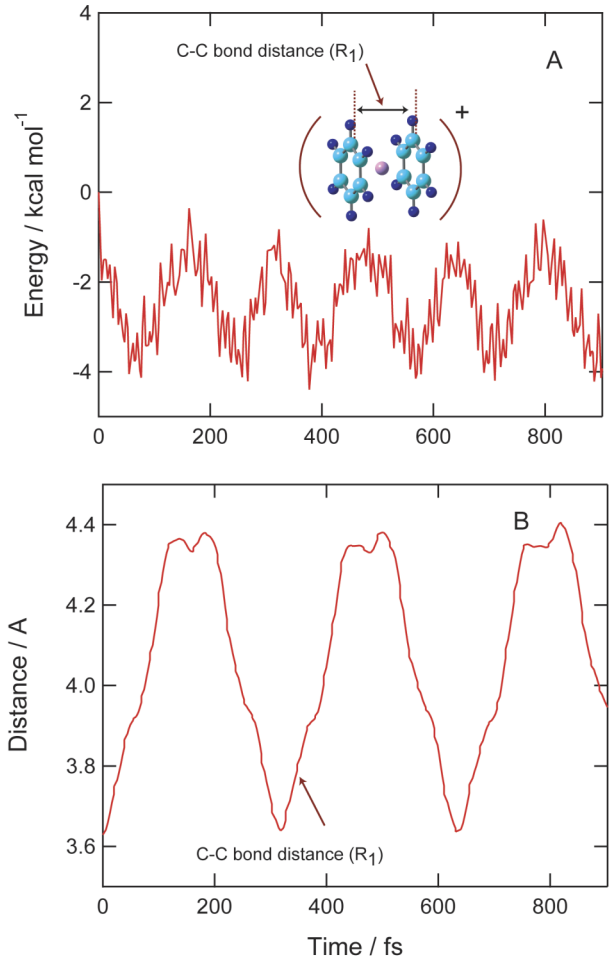

FIG. 6. Time evolutions of (a) potential energy of $Li^+(benzene)_2$ and (b) C–C bond distance between benzene rings of $Li^+(benzene)_2$ (R_1) following vertical hole capture from neutral state calculated as a function of time.

form. On the other hand, in distorted stacking form, the C–C bond formation was found at 900 fs. The time delay was caused by the rotation of benzene rings after the electron capture of $Li(Bz)_2$. Thus, the distortion of angle affects strongly on the reaction dynamics.

In actual system, the structure of $Li(Bz)_2$ fluctuates under thermal condition. The initial structure of $[Li(Bz)_2]_{ver}$ will be slightly varied from the equilibrium point of anion system $Li(Bz)_2$. To elucidate the effects of initial configurations on the reaction time for the C–C bond formation, several initial structures were selected and then the dynamics calculations were carried out with the same manner. The results were given in the supplementary material (Figure S1).[31] The reaction times for the C–C bond formation were distributed in the range of 250-450 fs, which are dependent on the distortion angle. However, all trajectories lead to the C–C bond formation as the product.

D. Hole capture dynamics

Time evolution of potential energy of the system $Li^+(Bz)_2$ following the hole capture (ionization) of $Li(Bz)_2$ is given in Figure 6. At short time propagation, the potential energy decreased to −1.8 kcal/mol due to the fast deformation of skeleton of benzene rings (~5 fs).

After the first structural stabilization, the potential energy of $Li^+(Bz)_2$ periodically fluctuated with several spikes. The time period of the long periodic vibration was estimated to be ca. 200 fs. Figure 6(b) shows time evolution of the C–C bond distance between benzene rings of $Li^+(Bz)_2$. The C–C bond distance between benzene planes fluctuated in the range of 3.62-4.40 Å. The structure of $Li^+(Bz)_2$ largely fluctuated: the time evolution of distance corresponds to a frequency of 105 cm^{-1}. The distance was 3.62 Å at time zero. After the hole capture, the distance increased rapidly and reached to the maximum value (4.40 Å) at 197 fs, and then, the distance was shortened to the 3.62 Å at 320 fs. Thus, the ionization of $Li(Bz)_2$ causes the periodic fluctuation of sandwich structure of $Li(Bz)_2$.

Time evolution of bond population between C_1 and C_2 atoms (P_{12}) after the hole capture was given in the supplementary material (see Figure S6).[31] At time zero, the population P_{12} was close to zero (−0.001). At time region of 100-200 fs, P_{12} was changed to positive. However, the value was almost zero during the reaction. These results indicate that the C–C single bond is not formed after the hole capture of $Li(Bz)_2$.

E. Energy diagram of electron capture process

The energy diagrams of electron capture processes of $Li(Bz)_2$ in gas phase and in acetonitrile are given in Figure 7. The zero level of energy in Fig. 7 corresponds to the total energies of reactants of $Li(Bz)_2$ in gas and in liquid phases. The vertical electron capture point in gas phase, $[Li^-(Bz)_2]_{ver}$, was 35.8 kcal/mol higher in energy than that of zero level. On the other hand, $[Li^-(Bz)_2]_{ver}$ in acetonitrile was 29.0 kcal/mol lower in energy than that of zero level. The results indicate that the electron affinity of $Li(Bz)_2$ becomes a positive in acetonitrile, and the electron capture process of $Li(Bz)_2$ takes place easily without activation barrier in liquid phase (acetonitrile).

After the electron capture of $Li(Bz)_2$ in gas phase, the energy of $[Li^-(Bz)_2]_{ver}$ decreased largely due to the structural relaxation from $[Li^-(Bz)_2]_{ver}$ to pre-complex (pre-comp). The parallel form of $[Li^-(Bz)_2]_{ver}$ was changed to the deformed form: the C–C bond distance between benzene planes was changed from 3.633 to 2.448 Å after the structural deformation. We found a transition state (TS) leading to the product state (PD). The inter-plane distances of TS and PD were calculated to be $R_1 = 2.114$ and 1.634 Å at the MP2/6-311++G(d,p) level, which is significantly shorter than $[Li^-(Bz)_2]_{ver}$ (3.633 Å).

The structural deformation of $[Li^-(Bz)_2]_{ver}$ causes a large stabilization energy (28.9 kcal/mol). Further deformation leads to TS of C–C bond formation of $Li^-(Bz)_2$. The activation energy of TS from pre-complex was 2.5 kcal/mol. The PD was 29.4 kcal/mol more stable than the energy level of $[Li^-(Bz)_2]_{ver}$. Hence, the C–C bond formation proceeds spontaneously after the electron capture of $Li(Bz)_2$. The vibrational frequency calculation of TS showed one imaginary

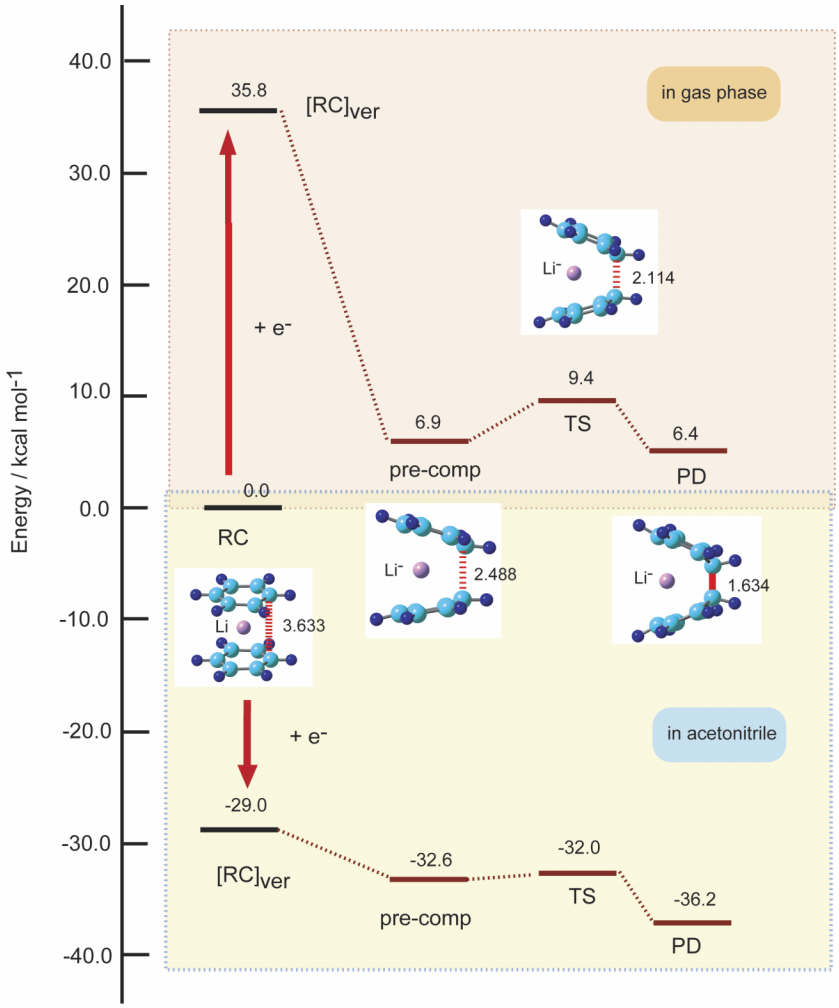

FIG. 7. Energy diagram of electron capture reaction of $Li(Bz)_2$ in gas phase (upper) and in liquid phase (acetonitrile) (lower). Values are relative energies (in kcal/mol) calculated at the MP2/6-311++G(d,p) level. The C–C bond distances are in Å.

frequency corresponding to the reaction for the C–C bond formation (227 $\boldsymbol{i}$ cm^{-1}). Details of the structure of TS, intrinsic reaction coordinate (IRC), and energy diagram are given in the supplementary material (see Figures S2, S3, and S4).[31]

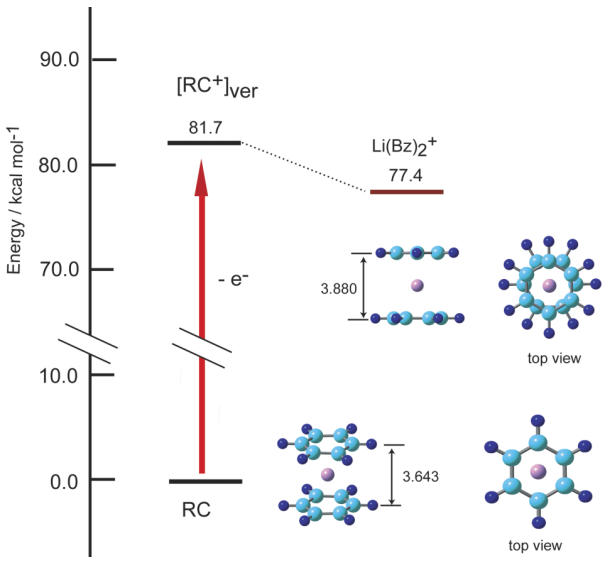

FIG. 8. Energy diagram of hole capture reaction of $Li(Bz)_2$ in gas phase. Values are relative energies (in kcal/mol) calculated at the MP2/6-311++G(d,p) level. The C–C bond distances are in Å.

The energy diagram of electron capture process in liquid phase was given in Fig. 7 (lower). The energy level of vertical electron capture point was 29.0 kcal/mol lower than that of zero level, indicating that the electron affinity of $Li(Bz)_2$ is positive in acetonitrile. The energy levels of pre-comp, TS, and PD were calculated to be −32.6, −32.0, and −36.2 kcal/mol. The shape of potential energy was composed of down-hill type. These results suggest that the benzene dimerization takes place easily in acetonitrile.

F. Energy diagram of hole capture process

The energy diagram of hole capture process of $Li(Bz)_2$ is given in Figure 8. The ionization potential of $Li(Bz)_2$ was calculated to be 5.46 eV, which is larger than that of free Li atom (5.34 eV). The vertical ionization point $[RC^+]_{ver}$ is 81.7 kcal/mol higher in energy than zero level. The ionization potential of Li atom was calculated to be 5.34 eV. The structure of $[RC^+]_{ver}$ will be relaxed to the stable form of $Li^+(Bz)_2$. The stabilization energy was calculated to be 4.3 kcal/mol, and the inter-plane distance was elongated from 3.643 to 3.880 Å.

G. Reaction mechanism

The orbital interaction of Li and benzene molecules is illustrated in Figure 9. First, the lithium and benzene 1:1

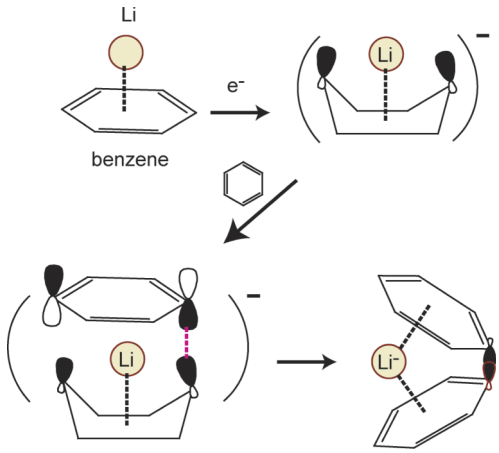

FIG. 9. Schematic illustration of orbital interaction and structural change of $Li(Bz)_2$ system following vertical electron capture of $Li(Bz)_2$.

complex was considered, and the structure was fully optimized at the MP2/6-31+G(d) level. Schematic illustration of the structure and the highest occupied molecular orbital (HOMO) of $[Li(Bz)]^-$ shows that the structure of $[Li(Bz)]^-$ has a boat form where lithium is located in the center of benzene ring. The HOMO is mainly localized in 1 and 4 carbon sites of benzene ring of $[Li(Bz)]^-$. When the second benzene molecule approaches the $[Li(Bz)]^-$, the lowest unoccupied molecular orbital (LUMO) of benzene molecule directly interacts with the HOMO of $[Li(Bz)_2]^-$. This interaction makes the new C–C single bond and the benzene dimerization proceeds smoothly without activation energy. Profile of potential energy shows a downhill type (Fig. 7): the C–C bond formation takes place spontaneously without the activation barrier.

IV. DISCUSSION

A. Comparison with previous experiment

Cooper and co-workers experimentally showed that dimerization of benzene molecules occurred by electrochemical two-electron reduction of $C_6H_6(Mn(CO)_3)^+$.[32] The reaction is schematically given in Figure 10. In the dimerization complex, the benzene molecules are connected by a C–C single bond. The mechanism of dimerization of $C_6H_6(Mn(CO)_3)^+$ is easily explained in terms of the present model. X-ray diffraction data of the dimer showed the C–C bond length between two benzene rings is 1.547 Å. This value is in reasonable agreement with the present calculations (1.634 Å).

TABLE II. Electron affinities of $Li(Bz)_2$ (EA in eV) in several solvents. The values were calculated at the MP2/6-311++G(d,p) level.

Solvent	EA/eV
None (*in vacuo*)	−1.55
Acetonitrile	1.27
Dimethyl sulfoxide	1.27
Tetrahydrofuran	1.00
Methanol	1.25
Water	1.29

B. Solvent effects on the electron capture process

Lithium atom has a positive electron affinity (0.68 eV)[33] in gas phase. The calculation used in the present study also gave the positive electron affinity of Li atom: 0.29 eV at the MP2/6-311++G(d,p) level. On the other hand, the electron affinity of $Li(Bz)_2$ showed a negative electron affinity due to the fact that the diffusive valence orbital of Li^- injected into the narrow space composed of two benzene rings. This result indicates that the reaction

$$Li(Bz)_2 + e^- \rightarrow [Li^-(Bz)_2]_{ver} \quad (1)$$

is essentially endothermic in gas phase.

To search the experimental condition in which reaction (1) proceeds exothermic, several solvents were examined for the calculation of electron affinity of $Li(Bz)_2$, and the energy differences were calculated at the MP2/6-311++G(d,p) level.

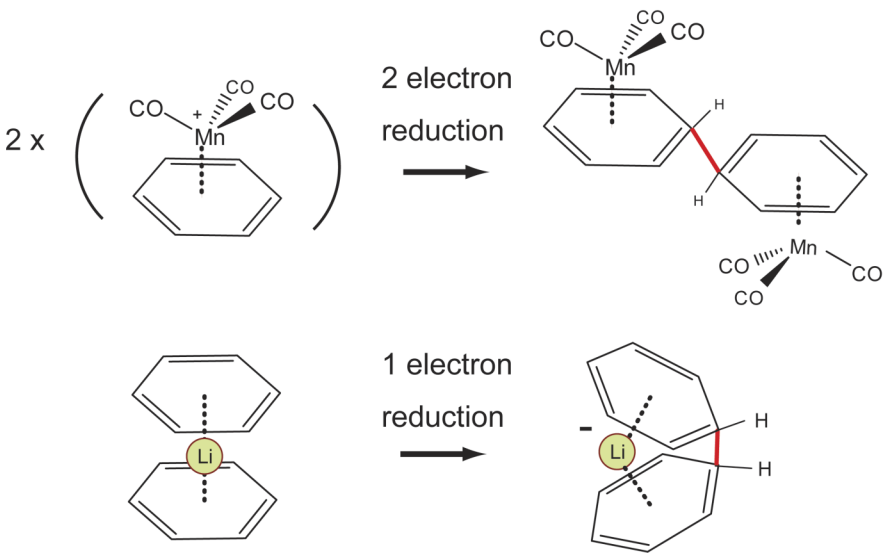

FIG. 10. Reaction schemes for benzene dimerization reactions. (Upper) 2-Electron reduction and (lower) one electron reduction (present study).

The energies of reaction (1) calculated in several solvents are given in Table II. In gas phase without solvent, the electron affinity of $Li(Bz)_2$ is −1.55 eV (negative). On the other hand, all electron affinities of $Li(Bz)_2$ in liquid phase showed positive values in the range of 1.0-1.29 eV. These results suggest that reaction (1) proceeds exothermic in several polar solvents.

C. Remarks

In the present study, the electron and hole capture processes of $Li(Bz)_2$ were investigated by means of direct AIMD method. This molecule is a smallest-sized model of lithium-graphite system. The calculations showed that the electron capture causes an attractive force between benzene rings, whereas the hole capture causes weak repulsive force. In actual system, the size of graphite is significantly larger than the present system. Hence, the electron capture does not give to the direct C–C bond formation. To elucidate the limitation of C–C bond formation, the larger sized-model will be needed.

In the present study, we considered only one structure of $Li(Bz)_2$: i.e., the sandwich structure of $Li(Bz)_2$. To search the other stable structure of $Li(Bz)_2$, several initial geometries were examined in the geometry optimization. We found one isomer of $Li(Bz)_2$, and the structure was given in the supplementary material (see Fig. S5).[31] The Li^- atom was located on the benzene plane of benzene dimer. The total energies of this form are, however, less stable by 22.1 kcal/mol than $Li(Bz)_2$, indicating that the most stable form is $Li(Bz)_2$ obtained from the direct AIMD calculation.

The trajectory of the reaction does not always proceed via the intermediate region. In addition, a reaction may not progress by thermal equilibrium. The present electron capture reaction occurred together with the generation of large heat of reaction. This suggests the possibility that the reaction proceeds in a nonequilibrium state. In the case of such a nonequilibrium reaction, the direct AIMD calculation becomes a powerful tool to elucidate the reaction mechanism. The direct AIMD calculation provides the time scale of the reaction and provides a reaction path to reach the product directly. Hence, we carried out the direct AIMD calculation in the present study. In the present system, the trajectory reached directly the product state and the lifetime of the pre-complex was negligibly small.

D. Conclusion

In the present study, the electron and hole capture dynamics of a lithium-benzene sandwich complex, expressed by $Li(Bz)_2$, have been investigated by means of direct AIMD method. Following the electron capture of $Li(Bz)_2$, the structure of $[Li(Bz)_2]^-$ was drastically changed: Bz–Bz parallel form was rapidly deformed and a new C–C single bond was formed in the C_1–C_1' position of Bz–Bz interaction system. In the hole capture, the intermolecular vibration between Bz–Bz rings was only enhanced. The mechanism of C–C bond formation in the electron capture was discussed on the basis of theoretical results.

ACKNOWLEDGMENTS

The author acknowledges partial support from JSPS KAKENHI, Grant No. 24550001, and MEXT KAKENHI, Grant No. 25108004.

[1]S. N. Mlynarski, C. H. Schuster, and J. P. Morken, Nature **505**, 386 (2014).
[2]Z. J. Quan, F. Q. Jing, Z. Zhang, Y. X. Da, and X. C. Wang, Eur. J. Org. Chem. **2013**, 7175.
[3]L. Xu, S. Y. Ding, and P. F. Li, Angew. Chem., Int. Ed. **53**, 1822 (2014).
[4]K. D. Hesp, D. P. Fernando, W. H. Jiao, and A. T. Londregan, Org. Lett. **16**, 413 (2014).
[5]T. L. Gianetti, R. G. Bergman, and J. Arnold, Polyhedron **84**, 19 (2014).
[6]M. A. Dufert, K. L. Billingsley, and S. L. Buchwald, J. Am. Chem. Soc. **135**, 12877 (2013).
[7]Y. Yamamoto, S. Takada, N. Miyaura, T. Iyama, and H. Tachikawa, Organometallics **28**, 152 (2009).
[8]M. M. Hansmann, M. Pernpointner, R. Doepp, and A. S. K. Hashmi, Chem. - Eur. J. **19**, 15290 (2013).
[9]T.-X. Zhang and Z. Li, Comput. Theor. Chem. **1016**, 28 (2013).
[10]C. Gourlaouen, G. Ujaque, A. Lledos, M. Medio-Simon, G. Asensio, and F. Maseras, J. Org. Chem. **74**, 4049 (2009).
[11]H. Tachikawa, Phys. Chem. Chem. Phys. **13**, 11206 (2011).
[12]H. Tachikawa, Theor. Chem. Acc. **132**, 1374 (2013).
[13]H. Tachikawa, RSC Adv. **2**, 12346 (2012).
[14]M. Li, X. H. Hou, Y. J. Sha, J. Wang, S. J. Hu, X. Liu, and Z. P. Shao, J. Power Sources **248**, 721 (2014).
[15]R. L. Woodin and J. L. Beauchamp, J. Am. Chem. Soc. **100**, 501 (1978).
[16]R. W. Taft, F. Anvia, J.-F. Gal, S. Walsh, M. Capon, M. C. Holmes, K. Hosn, G. Oloumia, R. Vasanwala, and S. Yazdani, Pure Appl. Chem. **62**, 17 (1990).
[17]J. C. Amicangelo and P. B. Armentrout, J. Phys. Chem. A **104**, 11420 (2000).
[18]S. Hoyau, K. Norrman, T. B. McMahon, and G. Ohanessian, J. Am. Chem. Soc. **121**, 8864 (1999).
[19]J. B. Nicholas, B. P. Hay, and D. A. Dixon, J. Phys. Chem. A **103**, 1394 (1999).
[20]D. Feller, D. A. Dixon, and J. B. Nicholas, J. Phys. Chem. A **104**, 11414-11419 (2000).
[21]S. Tsuzuki, M. Yoshida, T. Uchimaru, and M. Mikami, J. Phys. Chem. A **105**, 769 (2001).
[22]J. W. Caldwell and P. A. Kollman, J. Am. Chem. Soc. **117**, 4177 (1995).
[23]J. M. Vollmer, A. K. Kandalam, and L. A. Curtiss, J. Phys. Chem. A **106**, 9533 (2002).
[24]P. A. Denis and F. Iribarne, Chem. Phys. Lett. **573**, 15 (2013).
[25]T. A. Baker and M. Head-Gordon, J. Phys. Chem. A **114**, 10326 (2010).
[26]M. J. Frisch, G. W. Trucks, H. B. Schlegel, G. E. Scuseria, M. A. Robb, J. R. Cheeseman, G. Scalmani, V. Barone, B. Mennucci, G. A. Petersson, H. Nakatsuji, M. Caricato, X. Li, H. P. Hratchian, A. F. Izmaylov, J. Bloino, G. Zheng, J. L. Sonnenberg, M. Hada, M. Ehara, K. Toyota, R. Fukuda, J. Hasegawa, M. Ishida, T. Nakajima, Y. Honda, O. Kitao, H. Nakai, T. Vreven, J. A. Montgomery, Jr., J. E. Peralta, F. Ogliaro, M. Bearpark, J. J. Heyd, E. Brothers, K. N. Kudin, V. N. Staroverov, R. Kobayashi, J. Normand, K. Raghavachari, A. Rendell, J. C. Burant, S. S. Iyengar, J. Tomasi, M. Cossi, N. Rega, J. M. Millam, M. Klene, J. E. Knox, J. B. Cross, V. Bakken, C. Adamo, J. Jaramillo, R. Gomperts, R. E. Stratmann, O. Yazyev, A. J. Austin, R. Cammi, C. Pomelli, J. W. Ochterski, R. L. Martin, K. Morokuma, V. G. Zakrzewski, G. A. Voth, P. Salvador, J. J. Dannenberg, S. Dapprich, A. D. Daniels, O. Farkas, J. B. Foresman, J. V. Ortiz, J. Cioslowski, and D. J. Fox, Gaussian 09, Revision A.02, Gaussian, Inc., Wallingford, CT, 2009.
[27]J. M. Herbert and M. Head-Gordon, J. Chem. Phys. **121**, 11542-11556 (2004).
[28]K. D. Closser, O. Gessner, and M. Head-Gordon, J. Chem. Phys. **140**, 134306 (2014).
[29]J. R. Choudhuri and A. Chandra, J. Chem. Phys. **141**, 134703 (2014).
[30]A. Ramirez-Solis and L. Maron, J. Chem. Phys. **141**, 094304 (2014).
[31]See supplementary material at http://dx.doi.org/10.1063/1.4906944 for (1) the effects of initial structure on the reaction dynamics, (2) IRC and TS structure, (3) energy diagram for electron capture process, (4) structure of isomer of $Li(Bz)_2$, and (5) time evolution of population of $Li(Bz)_2^+$.
[32]S. Lee, S. R. Lovelace, D. J. Arford, S. J. Geib, S. G. Weber, and N. J. Cooper, J. Am. Chem. Soc. **118**, 4190 (1996).
[33]Atomic spectra data base in National Institute of Standards and Technology (NIST).